Geo-Mar Lett (2009) 29:233–248
DOI 10.1007/s00367-009-0137-7

ORIGINAL

Fluid expulsion features associated with sand waves on Australia's central North West Shelf

A. T. Jones · J. M. Kennard · G. A. Logan · E. Grosjean · J. Marshall

Received: 2 November 2008 / Accepted: 30 March 2009 / Published online: 23 April 2009

Abstract Multibeam swath bathymetric data collected in 95–120 m water depth on Australia's North West Shelf revealed two distinct populations of sand waves: a laterally extensive, low-amplitude composite form comprising superimposed dunes and ripples, and a laterally restricted form which has unusually high bedform heights and slopes. These large subaqueous sand waves comprise bioclastic ooid/peloid sand. Significantly, evidence of seabed fluid flow was detected in association with the high-amplitude sand waves. This evidence includes seabed pockmarks approximately 2–15 m in diameter imaged with side-scan sonar, tubular and massive carbonate concretions dredged from the seabed, and potential active venting of a fluid plume from the seabed observed during an underwater camera tow. Molecular and isotopic analyses of carbonate concretions collected from within pockmarks associated with the high-amplitude sand waves indicate that the fluids from which they precipitated comprise modern seawater and are not related to thermogenic fluids or microbial gases. The fluid flow is interpreted to be driven by macrotidal currents flowing over the relatively steep slopes of the high-amplitude sand waves. Pockmarks and carbonate concretions then develop where the interstitial flows are confined and focused by subsurface 'mounds' in a shallow seismic reflector.

Introduction

The central portion of Australia's North West Shelf (NWS) is a vast and relatively poorly understood carbonate province offshore Western Australia. The modern marine geology of the NWS has been documented by Jones (1973) and James et al. (2004), with both studies focusing on the surficial sediments. The seafloor across the mid-shelf environment is relatively flat but has dramatic relief in the form of large subaqueous sand waves (James et al. 2004). These sand waves are interpreted to be stranded coastal or shallow tidal structures, or the result of sediment transport and deposition associated with internal tides (James et al. 2004).

A recent marine survey to the central NWS aimed to contribute to the understanding of seabed environments over a restricted area of the shelf in approximately 100 m water depth (Fig. 1), as part of a broader study of potential natural hydrocarbon seepage (Jones et al. 2007). Active thermogenic hydrocarbon seepage has previously been identified on the northern NWS as bubble plumes and acoustic flares rising from pockmark fields and hard grounds (Brunskill et al. 2005; Jones et al. 2005a, b; Rollet et al. 2006). The intensity of fluid seepage was found to be tide related, the strongest periods of fluid release being correlated with low tides.

Pockmarks are shallow seabed depressions, typically up to several tens of metres across and less than 10 m deep, which are formed by the removal or erosion of sediment (Hovland and Judd 1988; Judd and Hovland 2007). They occur in a wide variety of environmental settings, usually in relatively fine-grained sediments. Pockmarks probably form through a variety of mechanisms, but they are typically interpreted to be the result of buoyant fluids (predominantly gases) rising through shallow strata with sufficient rates to mobilise the sediment on the seabed (Paull et al. 2002; Judd and Hovland 2007).

In this paper, we (1) describe the nature of the sand waves in the study area on the basis of multibeam swath and side-scan sonar data, (2) describe evidence for seabed

A. T. Jones (✉) · J. M. Kennard · G. A. Logan · E. Grosjean · J. Marshall
Geoscience Australia,
GPO Box 378, Canberra ACT 2601, Australia
e-mail: Andrew.Jones@ga.gov.au

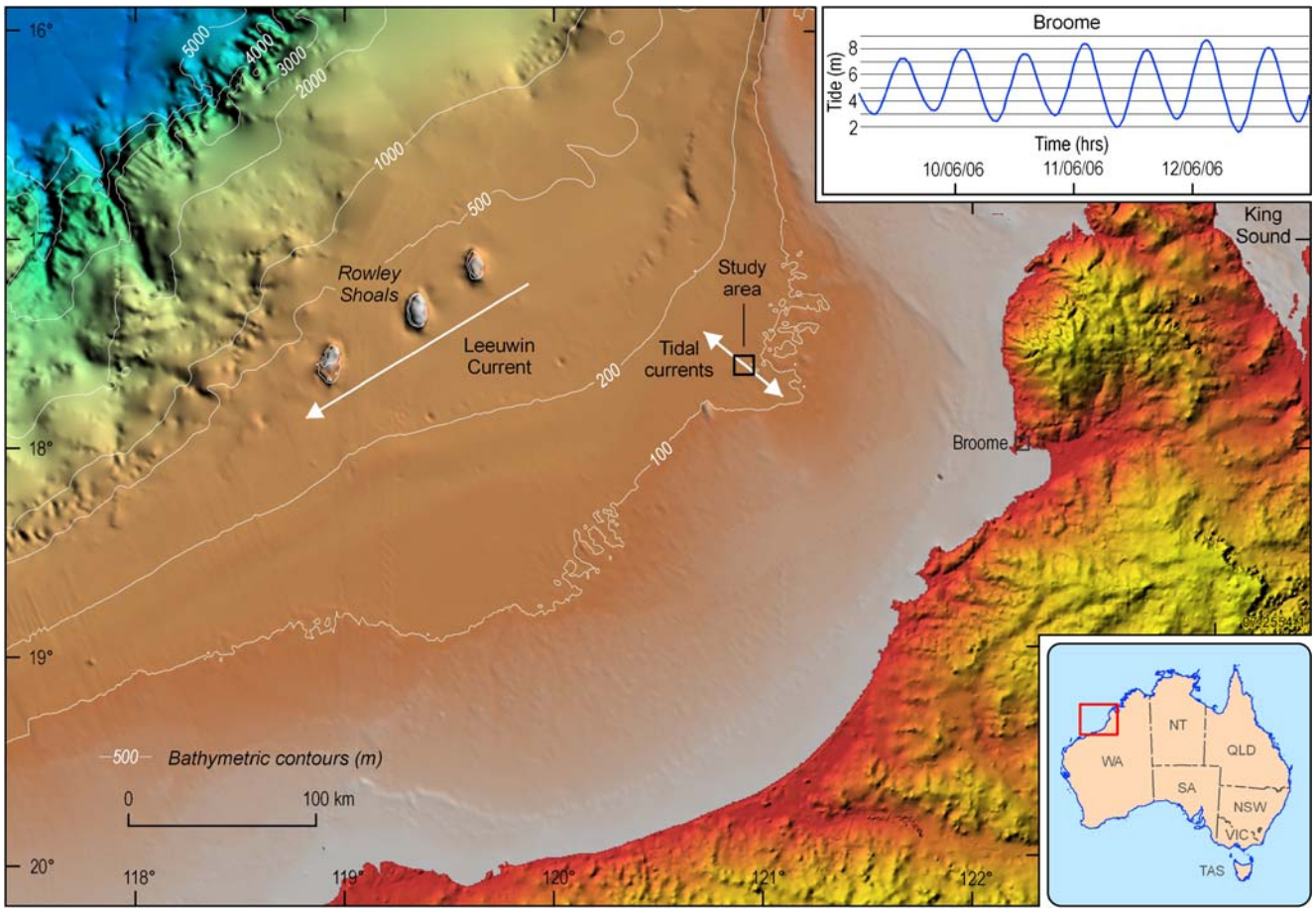

Fig. 1 Location of the study area, overlain on the bathymetry of the central North West Shelf. Tidal current orientation measured with an acoustic Doppler current profiler. Tidal magnitudes for the Broome tidal station calculated with XTide tidal prediction software. Orientation of the Leeuwin Current from Martínez et al. (1999)

fluid expulsion detected in acoustic data and seabed samples which were acquired during the marine survey, (3) assess the nature of the seeping fluid using geochemical and petrographic criteria and (4) discuss models for seabed fluid flow within the context of the modern sedimentary environment of the study area.

Physical setting

The central NWS covers approximately 165,000 km^2 offshore Broome, Western Australia (16–20°S and 118–122°E; Fig. 1). The central portion of the shelf is an ocean-facing carbonate ramp situated in a warm-water tropical setting adjacent to an arid hinterland of moderate to low relief (James et al. 2004). It is characterised by a gentle bathymetric ramp, ~250 km across at its widest point to the 200 m isobath (Fig. 1). The continental slope declines gradually from 200–1,000 m water depth over a distance of 60–100 km.

The NWS is a macrotidal shelf, where tidal ranges are above 4 m and attain 11.8 m in nearby King Sound (Fig. 1). Nearshore, the flood tide runs parallel to the shore but, further out towards the shelf edge, the ebb and flood tides run transverse to the shelf (James et al. 2004). Underway acoustic Doppler current profiler (ADCP) data acquired during the survey show that the tidal currents were flowing northwest-southeast in the study area (Fig. 1). Measured tidal current velocities during the flood phase reached 79 cm s^{-1} at 31 m water depth (~69 m above seabed) and 65 cm s^{-1} at 79 m water depth (~21 m above seabed). The maximum tidal current velocity during the ebb phase was 67 cm s^{-1} at both depths (Jones et al. 2007).

The Leeuwin Current dominates water circulation in this region (James et al. 2004). This is a warm (28–30°C), low-salinity (34–35‰) surface (<200 m deep) current which flows from the eastern part of the Indonesian Archipelago, around the western Australian coast to reach the Great Australian Bight in the Southern Ocean (Martínez et al. 1999). This tropical region is also characterised by periodic cyclone-generated storm winds, waves and currents.

The seafloor is strongly affected by the oceanographic factors listed above, resulting in preferentially accumulating

coarse-grained sediments (James et al. 2004). Previous research describes the sediments in the study area as mainly ooids and peloids (70–80%) with a few biofragments and 20–30% relict intraclasts (James et al. 2004). James et al. (2004) described the peloids from this region as faecal pellets, fillings of planktic foraminifers which were released by fracturing of the test, and rounded lithoclasts. The ooids from this region are described as commonly comprising a surficial coating on a peloid core, with only an occasional well-developed cortex. Radiocarbon dating of the ooids suggests that they formed over a narrow timeframe (15.4–12.7 ka), with incremental dating of the cortex indicating growth over ~2,000 years (James et al. 2004; Dix et al. 2005). Therefore, the ooids are interpreted to be 'relict' and to have formed on a shallow evaporative shelf during the transgression which followed the last glacial maximum (LGM), with formation arrested by the initiation of the less saline waters of the southward-flowing Leeuwin Current at approximately 12 ka (James et al. 2004). The continued exposure (i.e. lack of burial) of these relict ooids on the seabed, and the fragmented and reworked nature of the bioclasts, suggests that this area is a relatively high-energy environment with very low sediment input.

Materials and methods

The vessel used for the marine survey of the study area in June 2006 was the Australian National Facility Research Vessel *Southern Surveyor*. Surveying of the study area involved two primary operational components, a geophysical data acquisition component and a sampling component.

Geophysical data were acquired along nine parallel profiles oriented north-northwest, one perpendicular tie-line and two oblique intersecting lines, which map a seafloor coverage of approximately 4.6×9.1 km (Fig. 2). The data acquired were:

- swath bathymetric data collected by means of a Kongsberg Simrad EM 300 multibeam echo-sounder using 1° beamwidth and a nominal sonar frequency of 30 kHz, with a resulting lateral footprint between 1.75 m (inner beams) and 2.35 m (outer beams). Processed swath grids, tidally corrected using the record for Broome, provided a 3 m spatial resolution and <1 m vertical resolution of bathymetry;
- sub-bottom profile data collected using a Topas PU98 Parametric Sub-bottom Profiler, with a Ricker pulse at 1.5 kHz frequency and a ping interval of 450 ms;
- side-scan sonar data collected with an EdgeTech 4200-FS 120/410 kHz dual-frequency side-scan system. Generally, the sonar fish was operated at a frequency of 120 kHz in high-speed mode, at a speed of around 6 knots, and approximately 25–30 m above the seabed;
- single-beam echo-sounder data collected with a Simrad EK 500 system at 12 and 120 kHz frequencies.

The study area was sampled at four stations: four Smith-McIntyre sediment grabs, four rock dredges, and one deep underwater video camera tow (Jones et al. 2007). Between 0.5–1 kg of sediment from the Smith-McIntyre Grab was snap-frozen at −20°C for geochemical analysis; representative rock samples from each dredge were stored at 4°C. Gravity coring was attempted at three sites with a 6-m and then a 2-m core barrel; all were unsuccessful, due to the sandy nature of the substrate.

A selection of sub-samples from the dredges were examined petrographically and by means of X-ray diffraction (XRD) and scanning electron microscope (SEM) to investigate specific aspects of the sedimentology of the study area. A number of these samples were also analysed geochemically for their lipid composition to identify biomarkers related to potential natural hydrocarbon seepage.

The oxygen and carbon isotopic signatures of samples of aragonite cement and bulk ooid grainstone were measured using a Finnigan MAT 251 isotope ratio mass spectrometer equipped with a Kiel Carbonate Device. Individual ooids were disaggregated from the cemented grainstone with a stainless steel needle. The acicular aragonite cement was then mechanically separated from the ooid grains through agitation in a water suspension with a magnetic stirrer.

Results

Sand waves

The most striking feature from the multibeam swath bathymetry of the study area is the distribution of sand waves over the seabed (Fig. 2a). The sand wave crests are orientated roughly perpendicular to the local tidal currents (Fig. 1).

The relatively high resolution of the side-scan sonar data shows that the sand waves take on two forms (Fig. 3). Type I sand waves are composite features, comprising a series of smaller superimposed bedforms (Fig. 3a, c), which tend to be laterally extensive and of relatively low amplitude (Fig. 2a). In contrast, type II sand waves are smooth features, devoid of smaller-scale bedforms (Fig. 3b, d, e), and tend to be laterally discrete and of relatively high amplitude (Fig. 2a). Footage from the camera tow undertaken in the study area suggests that the type II sand waves are truly devoid of small-scale bedforms (Fig. 4a), not covered by bedforms below the resolution of the side-scan sonar. Small-scale

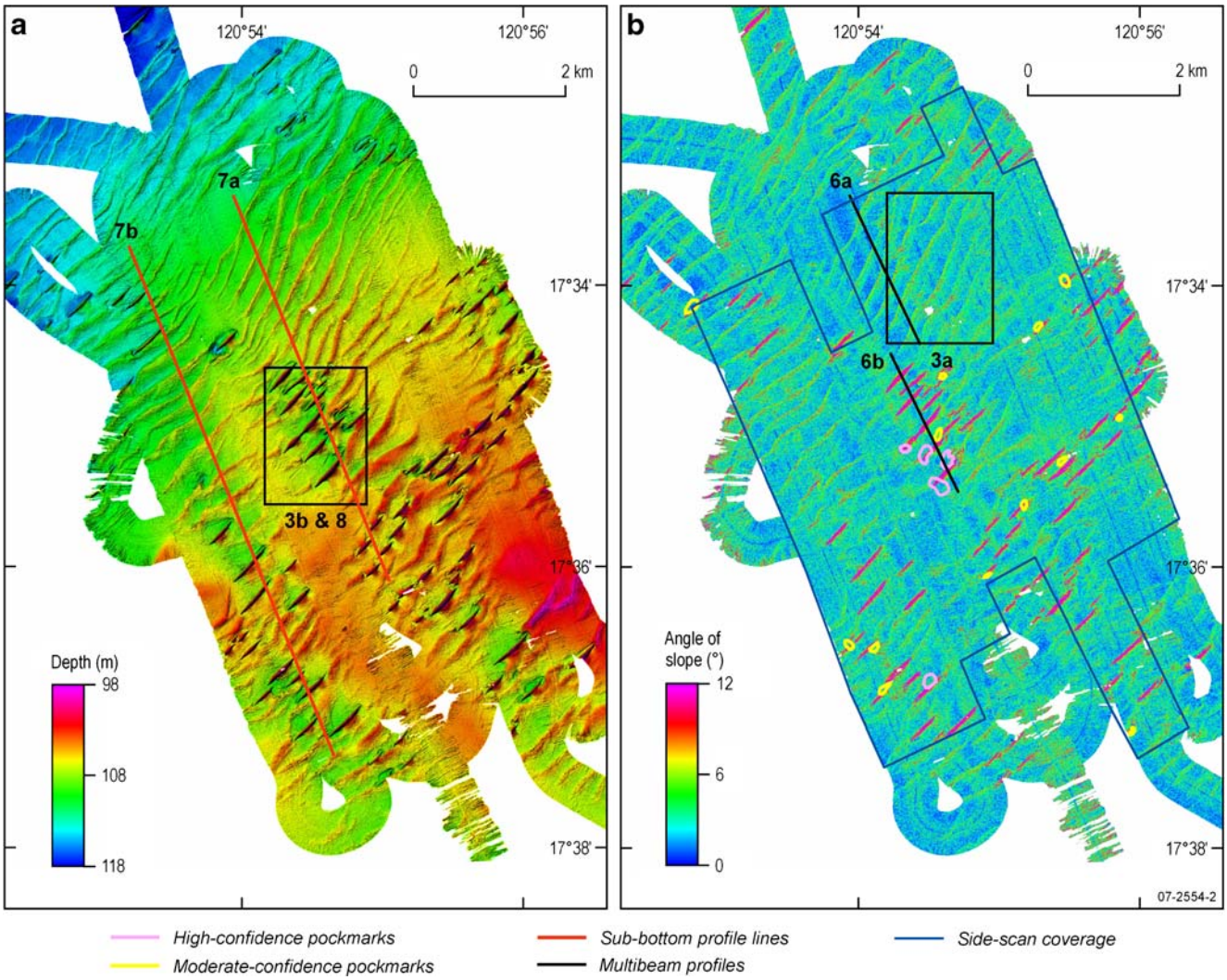

Fig. 2 **a** Multibeam swath bathymetry of the study area showing two types of sand waves; a low-amplitude laterally extensive form (type I) and a high-amplitude laterally restricted form (type II). **b** Slope map derived from the multibeam swath bathymetry. Type I sand waves are characterised by gentle slopes (~5°, *green and yellow tones*) relative to type II sand waves (~12°, *red and pink tones*)

gravity flows were visible at the crest of the type II sand waves (Fig. 4b).

A slope map derived from the multibeam bathymetry (Fig. 2b) displays the spatial distribution of the sand waves forms, with the laterally restricted type II sand waves characterised by higher slopes (~12°, corresponds to red and pink tones) relative to the more laterally extensive type I sand waves (~5°, corresponds to green and yellow tones).

The morphological elements of 20 examples of each sand wave type were measured to quantify the differences between these two populations (Table 1). A graph of sand wave slopes, providing evidence of two discrete populations of sand waves, is shown in Fig. 5a. In Fig. 5b, the sand wave length and height are also compared with a 'global' population of flow-transverse bedforms (Flemming 1988).

Key results from the morphological element analysis include:

- The type I sand waves are of significantly lower amplitude than the type II sand waves (Fig. 5b). The maximum height of a type I sand wave is 4.3 m, which is less than half the maximum height of a type II sand wave (9.2 m).
- The type I sand wave slopes (max. 6.3°) are significantly less than the type II sand wave slopes (max. 16.5°; Fig. 5a). Both sand wave types have steeper northwest-facing slopes relatively to southeast-facing slopes. The average modified symmetry index (stoss-side length/lee-side length-1; Allen 1980) for the type 1 sand waves is 0.66, and that for the average type II is 0.42.
- The height and length of the type I sand waves are in the vicinity of the global relationship as defined by Flemming (1988), whereas the type II sand waves plot

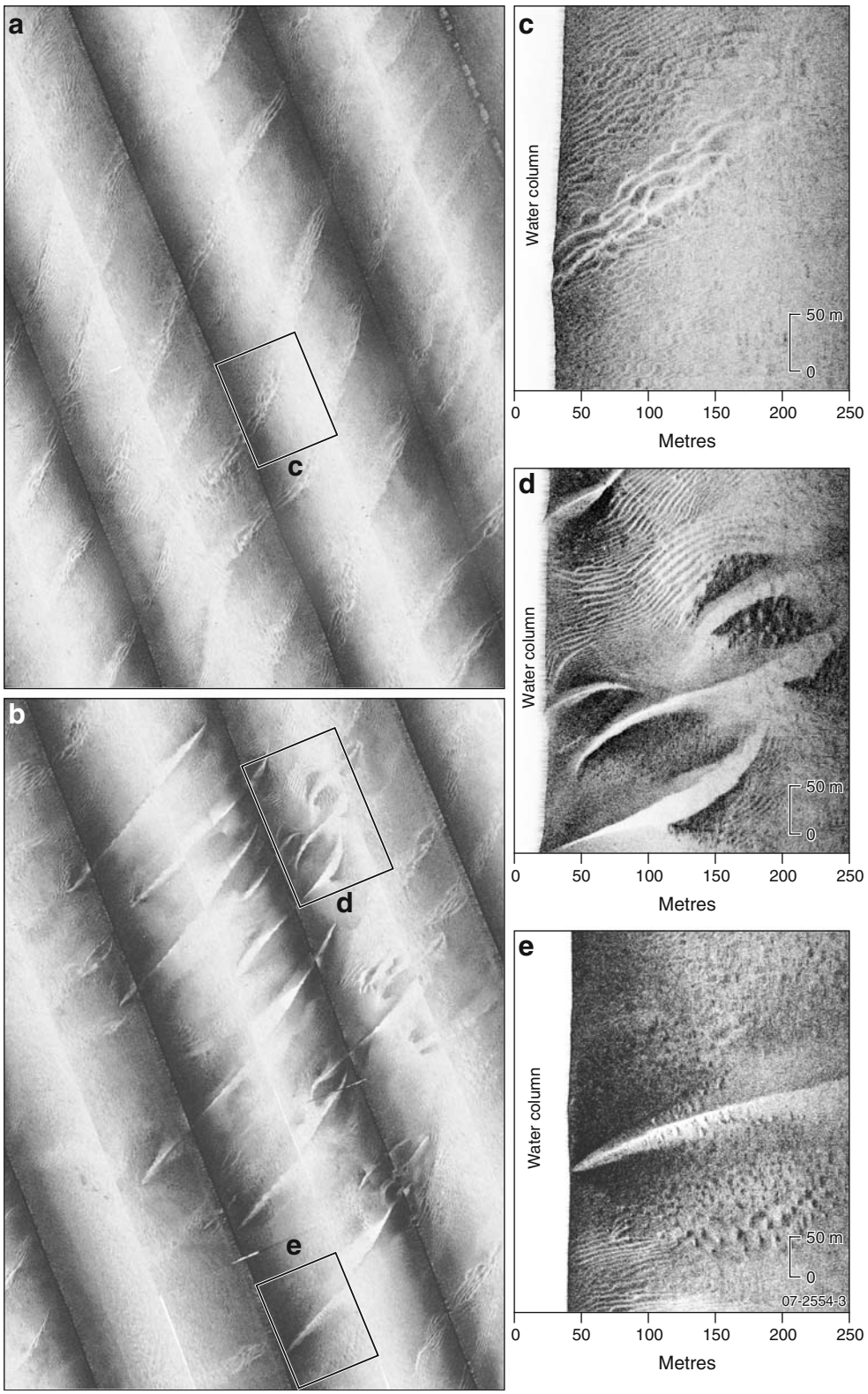

Fig. 3 **a** Side-scan sonar mosaic showing type I sand waves. **b** Side-scan sonar mosaic showing predominantly type II sand waves. Location of mosaics shown in Fig. 2. **c** Side-scan sonar track showing the composite nature of a type I sand wave, which comprises multiple smaller bedforms. **d** Side-scan sonar track showing type II sand waves devoid of smaller bedforms, and some moderate-confidence pockmarks. **e** Side-scan sonar track showing a type II sand wave and high-confidence pockmarks. Note the pockmarks penetrating the sand wave. *Dark areas* are high backscatter features; insonification is from the left in **c**–**e**

around and above the typically observed limit of the upper height limit relationship (Fig. 5b).

– The average vertical form index (VFI: wavelength/height; Bucher 1919) for the type I sand waves is 43.8 (range 31.5–59.0), whereas that for the average type II is 13.5 (range 10.0–21.9).

These key results show that the two sand wave forms are distinctly discrete populations, with type II sand waves

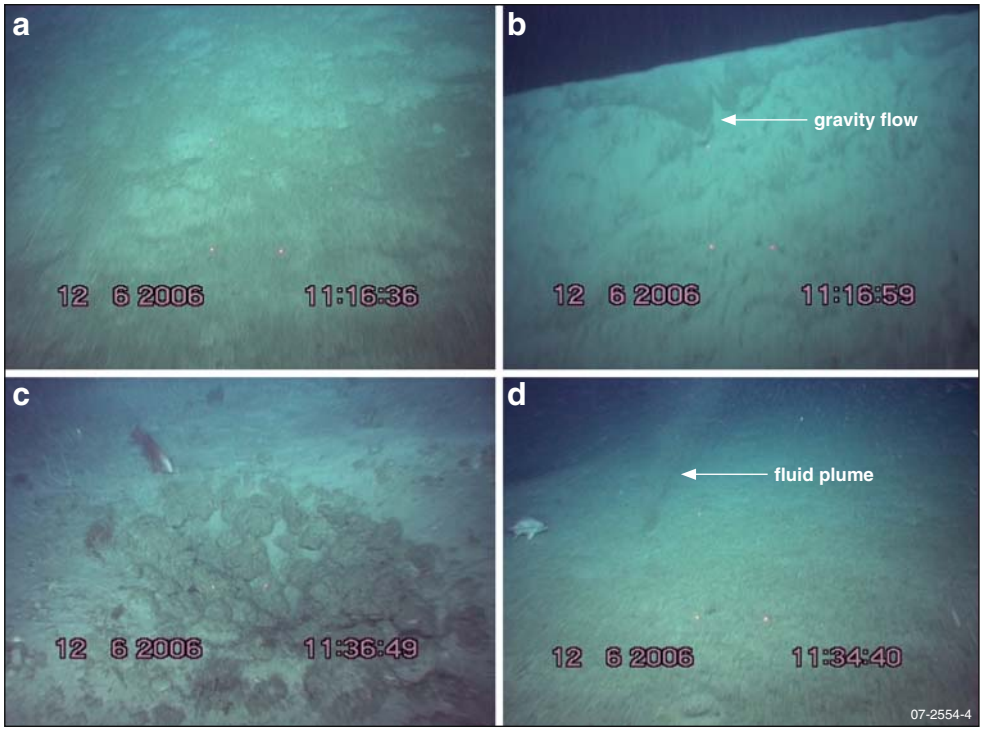

Fig. 4 Seabed photographs showing **a** the side of a sand wave which is devoid of small-scale bedforms; **b** the crest of a sand wave with small-scale gravity flows; **c** a small pock-mark with a lining of carbonate concretions; **d** what appears to be a fluid plume, potentially formed through active venting at the seabed. Seabed photographs taken in the vicinity of the type II sand waves in Fig. 3e. Laser points 25 cm apart

being significantly higher and steeper than type I sand waves.

Figure 6 shows profiles through type I and type II sand waves extracted from the multibeam bathymetry, and Fig. 7 shows sub-bottom seismic sections through the sand waves in the study area. These profiles show that the majority of sand waves are asymmetrical with a lee side to the northwest, but this asymmetry is amplified by the vertical exaggeration of the profiles. There is no obvious consistent cross-stratification within these sand waves based on the sub-bottom profile data. This indicates that the sand waves are devoid of coherent internal structure, or that sedimentary structures within the sand waves are below the resolution of the sub-bottom profiler system. The stratigraphy underlying the sand waves is characterised by a relatively continuous near-surface reflector (Fig. 7).

Table 1 Average bedform crest length (B), wavelength (L), height (H), vertical form index (VFI), horizontal form index (HFI), stoss-side length (A), lee-side length (B), modified symmetry index (MSI), maximum stoss-side slope (X), and maximum lee-side slope (Y) for measured sand waves (n=20 for each sand wave type)

	Type 1 sand waves	Type II sand waves
B (m)	1,306	402
L (m)	133	90
H (m)	3.1	6.7
VFI	43.8	13.5
HFI	10.2	4.7
A (m)	80.2	47.4
B (m)	53.2	42.2
MSI	0.66	0.42
X (°)	3.0	8.8
Y (°)	5.0	12.3

Pockmarks

Side-scan sonar data from the study area reveal seabed features which are roughly circular in shape and approximately 2–15 m in diameter, with higher backscatter in the far range and lower backscatter in the near range indicating that they have negative relief (Fig. 3e). These depressions on the seabed occur with a semi-regular spacing in sub-circular clusters. Footage from the camera tow, which traversed the cluster of crater-like features in Fig. 3e, showed that the depressions are constructed in unconsolidated sand but that some are lined with carbonate concretions (Fig. 4c).

The spatial distribution of the depressions was mapped on the basis of the side-scan sonar data (Fig. 2). Two interpreted confidence levels were mapped: high-confidence features (Fig. 3e) for which the negative-relief, crater-like morphology was clearly evident, and moderate-confidence features which were more ambiguous (Fig. 3d). The mapped spatial distribution in Fig. 2b shows that in every case the features are found in association with type II sand waves. Additionally, sub-bottom profile data indicate that, in at least some parts of the study area, the depressions

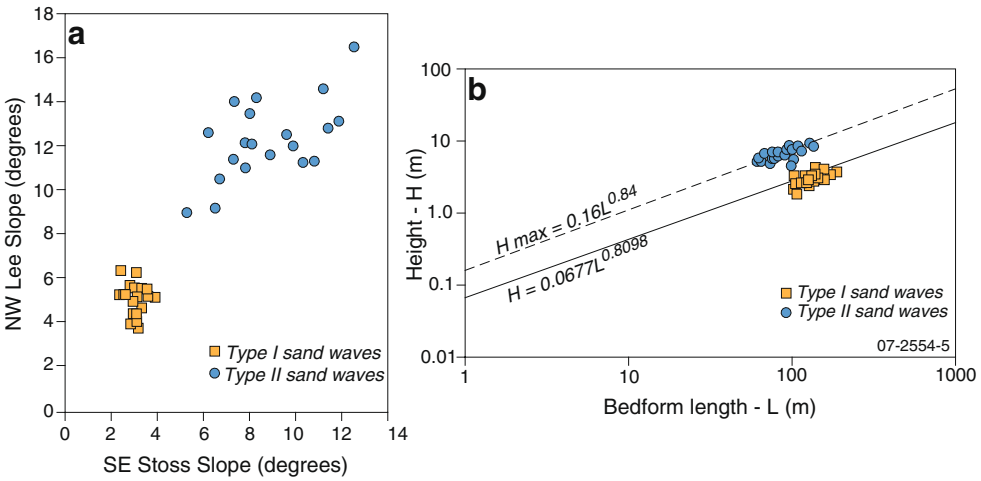

Fig. 5 **a** Lee vs. stoss slopes of sand waves, showing that type II sand waves are distinctly steeper than type I sand waves. **b** Global and upper height limit relationships for submarine sand waves from measurements of 1,491 subaqueous marine bedforms (Flemming 1988). Note that the type I sand waves plot on and around the global average, whereas most of the type II sand waves plot around and above the upper height limit

are located adjacent to type II sand waves which overlie subsurface 'mounds' in the near-surface reflector. Figure 7a and the southern end of Fig. 7b show the location of depressions in the vicinity of type II sand waves which are over a mound in the reflector, but no depressions are situated near the type II sand wave towards the centre of Fig. 7b, where the reflector is relatively deep.

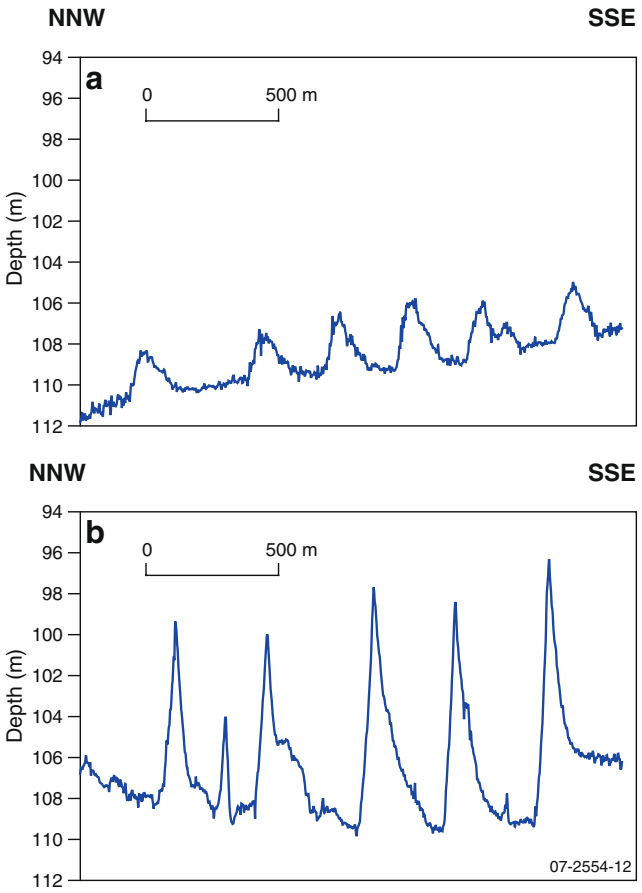

Fig. 6 Seabed profiles extracted from multibeam swath bathymetry displaying the cross-sectional geometries of type I sand waves (**a**) and type II sand waves (**b**). Location of profiles shown in Fig. 2b

Fluid plume

The camera tow showed what appears to be a vertical plume of fluid extending from the seabed (Fig. 4d), which persisted from the time that it appeared in the field of view until it was bypassed by the camera (ca. 5 s). In Fig. 4d, the plume is 2-3 m from the camera and appears to be >1 m in height. The fluid plume is interpreted to have formed through active venting at the seabed, i.e. the same process leading to the development of pockmarks. The fluid plume is unlikely to have represented an organism such as a worm or clam 'blowing' out of a burrow, as it was too large and persistent in time. The camera did not impact the seabed during this section of the traverse; therefore, it does not represent flow induced by impact pressure. The plume superficially resembles a current eddy; however, the discrete nature of the feature and the lack of a correspondingly discrete seabed bathymetric feature adjacent to the plume suggest that it is not a current eddy.

Seabed sediments

The seabed sampling program was part of a regional reconnaissance study of natural hydrocarbon seepage on the broader central North West Shelf; therefore, only four grab samples were collected in the study area. The sediment recovered from the grabs comprised bioclastic ooid/peloid sand. The sand contents exceeded 82% of the bulk sediments, and the carbonate contents were approximately equal to or greater than 90%. In addition to the dominant ooid/peloid component, there was a minor but diverse biogenic component which was moderately fragmented and reworked.

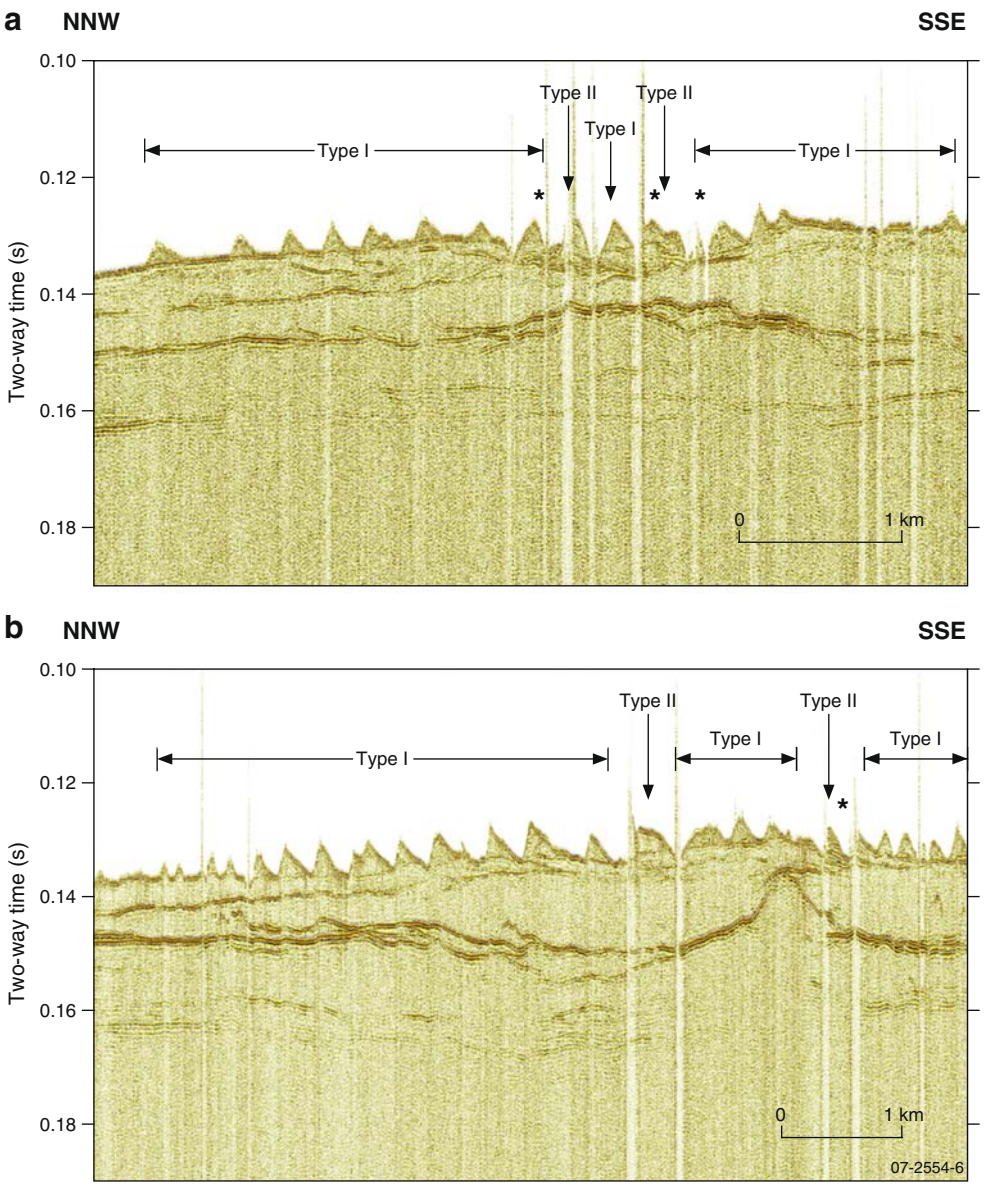

Fig. 7 Sub-bottom profile lines showing the shallow stratigraphy of the study area. Type I and type II sand waves were classified on the basis of side-scan sonar data (Fig. 3). Vertical stripes through the data are noise introduced when the profiler loses bottom tracking, typically on the steep slopes of type II sand waves. *Asterisks* show pockmark sites identified in side-scan sonar data for these transects. Twenty milliseconds two-way time is equivalent to approximately 15 m. Locations of lines shown in Fig. 2a indicate that the profiles intersect only the extremities of some sand waves

Figure 8 shows a detailed grain-size distribution of the sand fraction, determined through laser grain-size analysis. Three of the grab samples, collected from troughs between the sand waves, display a very similar distribution with a dominant mode at approximately 500 μm and a lesser mode at approximately 125 μm (the coarse- to medium-grained sand and fine- to very fine-grained sand fractions represent biogenic components and ooids/peloids respectively). The remaining grab sample, recovered from a type II sand wave, displays the same modes but the 125 μm mode is dominant. Therefore, the type II sand waves appear to be composed of finer sand than the 'interdune' areas where the other grabs were taken, with a corresponding higher proportion of ooids and peloids relative to biogenic debris. A similar relationship has been observed for sand waves in the Irish and North seas, with finer material on the crests relative to the troughs (Harvey 1966; Terwindt 1971).

Carbonate concretions

A number of dredges returned a variety of ooid grainstones, which are interpreted to be similar to the carbonate concretions seen lining the pockmark in Fig. 4c. Tubular concretions were recovered from the dredges. These tubes varied between very simple forms (Fig. 9a) to complex irregular tubes with openings up to 4 cm in diameter (Fig. 9c, d). Irregular, massive carbonate concretions, an example of which is shown in Fig. 9b, were also recovered from the dredges.

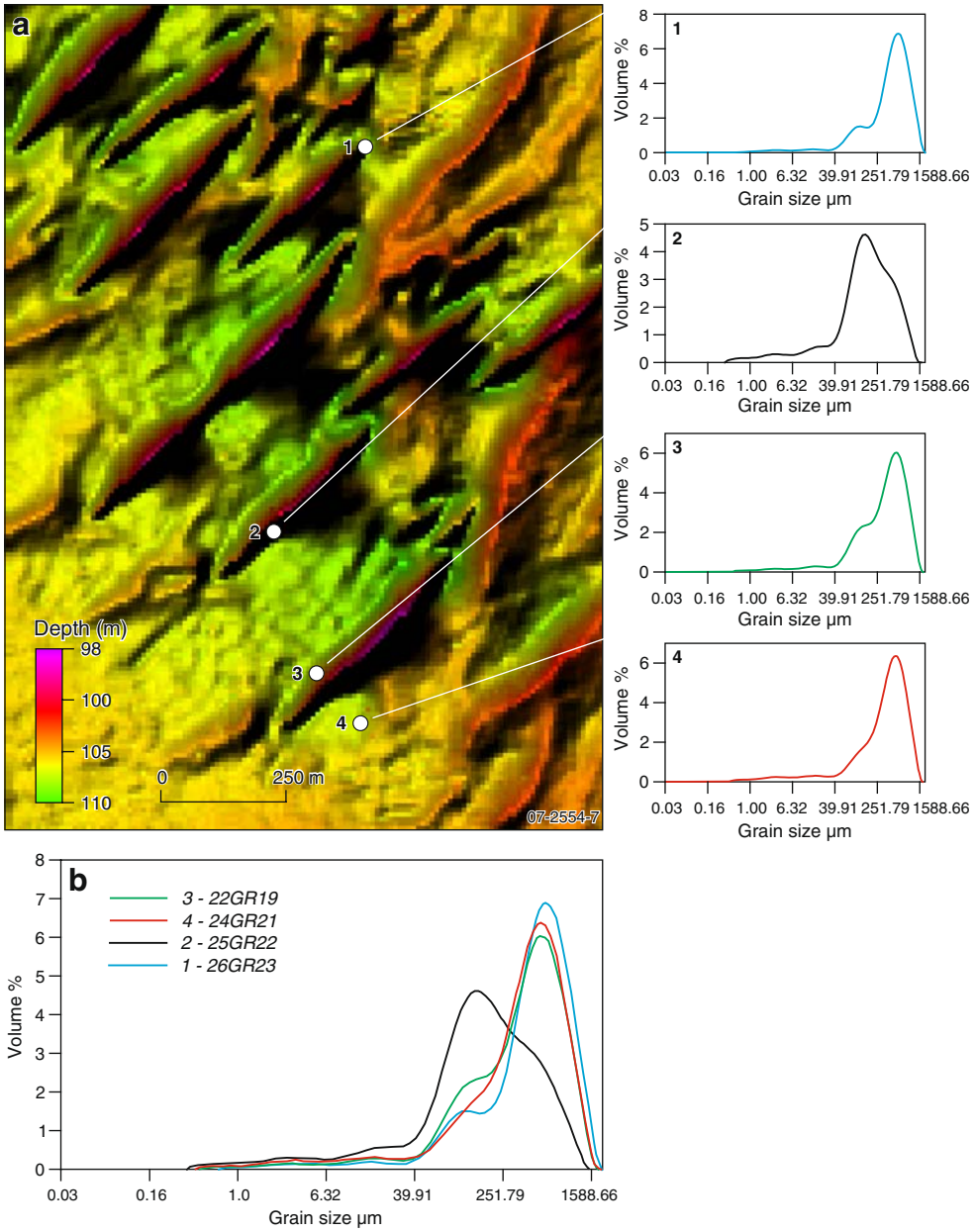

Fig. 8 **a** Location and grain size of grab sample sediments in the vicinity of type II sand waves. **b** Comparison of sediment grain sizes in the grabs. Line styles correspond to insets in **a**

Petrographic analyses of the tubes and massive concretions show that they comprise grainstone with ooids and pellets making up the majority of the sample. The ooids range from 150–750 µm in diameter; most are made up of the pellet or skeletal nucleus with the cortex generally forming a surficial layer of only 10–20 µm (Fig. 10). Some of the ooids have a thicker cortex, up to about 200 µm thick (e.g. top left ooid in Fig. 10a), where the concentric layering is more obvious. The pellets and surficial ooids have been cemented by acicular aragonite cement which forms an isopachous fringe <10–50 µm thick (Fig. 10).

SEM analysis shows the pellets and ooid nuclei to comprise (sub)microcrystalline carbonate (Fig. 10b, c). The concentric layers in the ooid cortex consist of randomly oriented equi-dimensional crystals (Fig. 10c). In contrast, the fringing cement comprises acicular crystals orientated perpendicular to the ooid cortex/nucleus surface (Fig. 10c).

XRD records from these samples are dominated by aragonite (75–89%), with only minor proportions of Mg-calcite (9–21%) and calcite (1–4%); the latter are contributed mainly by benthic foraminifers and echinoids (Mg-calcite) and planktonic foraminifers (calcite).

Geochemistry

The oxygen and carbon isotopic signatures of aragonite cement and bulk ooid grainstone from one of the carbonate concretions were examined in order to determine potential

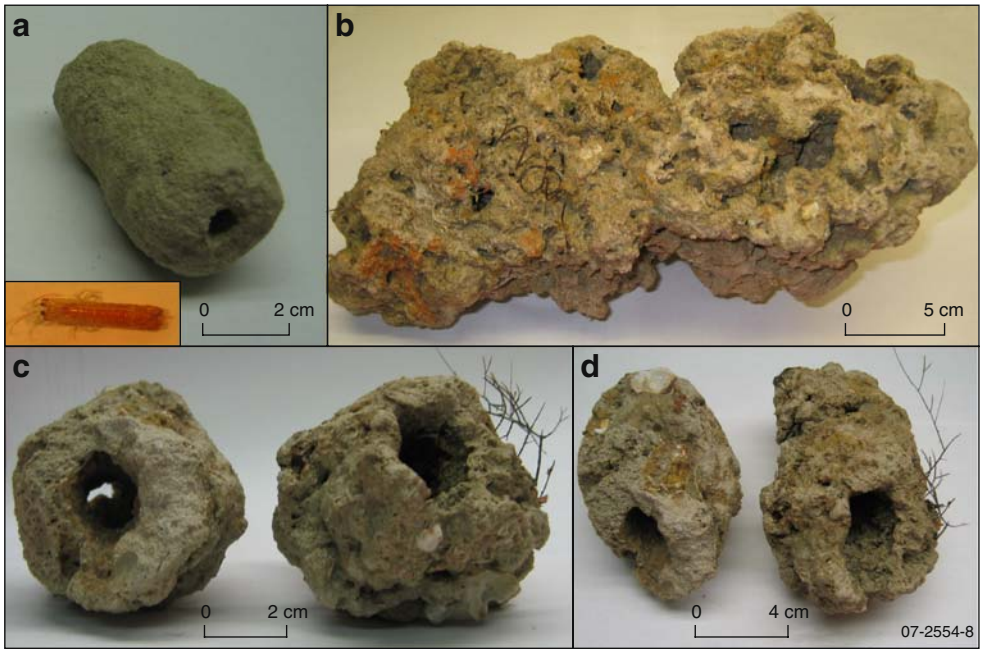

Fig. 9 Carbonate concretions recovered from dredges in the study area. **a** Relatively small, simple tube. The shrimp in the inset was recovered from the tube. **b** Irregular massive concretion. **c**, **d** Tubular concretions which have formed from fluid expulsion near the seabed

sources of diagenetic fluid which may have cemented the sediment. The average $\delta^{13}C$ isotope values for the bulk grainstone and acicular aragonite crystals were 4.01 and 3.46‰ respectively. The average $\delta^{18}O$ isotope values for the bulk grainstone and acicular aragonite crystals were 0.52 and 0.13‰ respectively (all values are normalised to Vienna-Pee Dee Belemnite (V-PDB) scale and duplicates were within ±0.03‰ maximum).

Very distinct biomarker assemblages are commonly found in methane-derived carbonate build-ups and provide evidence for anaerobic oxidation of methane (AOM) processes and, hence, for methane seepage. Examples of typical compounds are dialkyl glycerol diethers, archaeol and hydroxyarchaeols, as well as irregular isoprenoids crocetane and 2-, 6-, 10-, 15-, 19-pentamethylicosane (PMI), all reflecting the presence and metabolic activity of methanotrophic archaea involved in AOM (Elvert et al. 2000; Thiel et al. 2001; Aloisi et al. 2002; Pape et al. 2005; Reitner et al. 2005). However, biomarkers related to AOM were not found within the carbonate concretions. Additionally, high-molecular weight petrogenic hydrocarbons or any unresolved complex mixture related to their biodegradation were not detected within any of the concretions.

Discussion

Sand waves

The sand wave crests are orientated roughly perpendicular to the local tidal currents, which is typical for sand waves; the orientation of the wave crest tends to be within 10° of perpendicular to the principal tidal current direction (Van Veen 1935; McCave 1971; Hulscher 1996; Németh et al. 2002). This suggests that their formation is associated primarily with tidal currents across this part of the shelf, with relict sediments worked back and forth and producing little net movement, and that these sand waves are unlikely to represent stranded coastal or shallow tidal structures (cf. James et al. 2004).

The absence of small-scale bedforms indicates either that no current-driven sediment movement is occurring on the

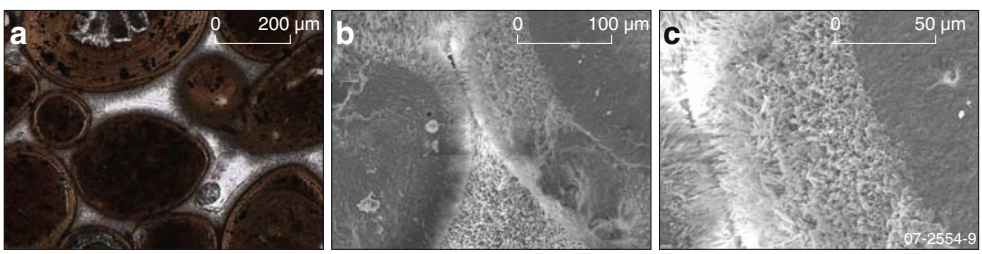

Fig. 10 Photomicrograph (**a**) and SEM images (**b**, **c**) of ooid grainstone showing surficial ooids and pellets which have been cemented by fine fringes of acicular aragonite cement

faces of type II sand waves, or that sediment movement is in the plane bed phase. Small-scale gravity flows were visible at the crest of the type II sand waves (Fig. 4b). These sand waves may therefore be somewhat anomalous in this context, as the low slopes of typical sand waves generally confine sediment avalanching to superimposed smaller-scale bedforms (Allen 1982). The anomalous nature of the sand waves is highlighted in that:

1. Allen (1982, p. 457) states: "We cannot emphasize too strongly that sand waves possess low to mild slopes ... the sides of the waves rarely dip more steeply than 10° overall and can slope as little as 1°". The average type II sand wave slope is approximately 10°; therefore, the slopes of sand waves are steeper than those generally associated with this bedform (Harris et al. 1986; Ashley et al. 1990).
2. The VFI of sand waves is generally between 20 and 100 (Allen 1982; Ashley et al. 1990; Hulscher and Van den Brink 2001; Németh et al. 2004, 2007). The average VFI of the type I sand waves is mid-way through the 'typical' range but the average VFI of the type II sand waves is below the low range value, and lower than the values for the giant sand wave field in Long Island Sound (Fenster et al. 2006).
3. The heights of most of the type II sand waves plot above the typically observed limit (relative to length) for flow-transverse bedforms based on the observations of Flemming (1988) and the review of Ashley et al. (1990).

Only four seabed samples were collected in the study area and none in the vicinity of type I sand waves. Differences in sediment grain size may account for the presence of two sand wave populations, but more detailed seabed sampling is required in order to address this potential hypothesis.

Pockmarks

The size, frequency, semi-regular spacing and clustering of the seabed depressions, and the remoteness of the study area from population centres, suggest that they formed through a physical, rather than biological or anthropogenic process. The crater-like nature of the depressions strongly suggests that they are erosional features; therefore, they are likely to represent sinkholes or pockmarks. Underwater video observations of the seabed (Fig. 4), physical samples collected with the grab (Fig. 8), and the generally low backscatter response in side-scan sonar data (Fig. 3) showed the erosional features to occur within unconsolidated sediments. The depressions are therefore interpreted as pockmarks, which form when buoyant fluids migrate upwards through shallow strata with sufficient rates to mobilise the unconsolidated sediment on the seabed (Judd and Hovland 2007).

A sinkhole interpretation is not favoured for these features, despite the carbonate environmental setting in the study area being consistent with karstic processes:

- The study area depressions would represent small-scale sinkholes distributed in close proximity to one another (cf. Land and Paull 2000). If the features had formed through carbonate dissolution, then at least some would be expected to have coalesced into large-scale collapse structures similar to the sinkholes in the Straits of Florida, which are hundreds of metres in diameter and at least 30 m deep (Land et al. 1995; Land and Paull 2000).
- Sand waves in the study area record a history of sediment mobilisation and accumulation. It is unlikely that the depressions formed as sinkholes during the LGM lowstand, as they would have been infilled by sediment during the Holocene.
- In some cases the depressions occur in the unconsolidated sand waves (Fig. 3e). It is unlikely that the depressions existed prior to sand wave development (as they would have been infilled with sediment) and it is similarly improbable that formation of sinkholes in a consolidated karstic surface beneath an existing sand wave would lead to a series of individual depressions on the face of the bedform.

Carbonate concretions

The process of carbonate cement formation is not clear, based only on concretion morphology. Some of the simple tubes are likely to have been formed by marine invertebrates (Fig. 9a), as indicated by the presence of biota within the sampled concretions. The irregular massive concretions and the larger complex tubes closely resemble authigenic carbonate tubes and slabs formed through seabed fluid venting in the Gulf of Cadiz and the North Sea (Díaz-del-Río et al. 2003; Judd and Hovland 2007). Based on the interpretation of fluid expulsion pockmarks in the study area, the sampled concretions may have also formed through this mechanism. If this is the case, then it is possible that the massive concretions recovered from the study area are an evolution of the tubular structures in Fig. 9c, d; as the tubes develop and grow, the openings fill with cement and massive concretions are formed (cf. Judd and Hovland 2007).

The petrography and mineralogy of the ooid grainstone cements from the study area are similar to those of aragonitic submarine cements comprising isopachous fringes of acicular crystals recovered from approximately 2 m below the surface of bioclastic sand dunes in Torres Strait (Keene and Harris 1995).

The nature of the seeping fluid

A diverse range of fluids create expulsion features as they flow through the seabed. Examples include hydrothermal fluids (Fyfe 1994; Butterfield 2000), submarine groundwater discharge (Taniguchi et al. 2002; Burnett et al. 2003) and expelled basinal porewaters (Dugan and Flemings 2000, 2002), but the most widely documented seeping fluids are rich in biogenically or thermogenically generated hydrocarbons, which are in general dominated by methane (Hovland and Judd 1988; Judd and Hovland 2007).

Methane seepage is typically detected through the analysis of headspace gas in seabed sediments from core samples. It was not possible to analyse the nature of the seeping fluids in the study area using this method, due to the lack of recovery in deployed seabed cores. Seepage of methane through shallow substrata can be detected as amplitude anomalies, acoustic blanking or turbidity in sub-bottom profiler data (Hovland and Judd 1988; Judd and Hovland 2007). However, no evidence of shallow gas was identified in the 1.5-kHz Topas data (Fig. 7), as was the case in the Arafura Sea where pockmarks were discovered in association with anomalies in sub-bottom profile data (Rollet et al. 2009). Similarly, bubbles were not acoustically identified in the water column with the side-scan sonar or single-beam echo-sounder, as detected above hydrocarbon seepage sites on the northern NWS (Rollet et al. 2006). The absence of water column flares could be explained by the episodic nature of seepage, although acoustic surveying of the pockmark sites was undertaken at low tide to maximise the probability of detecting active seepage. The absence of gas seepage indicators in the acoustic datasets is consistent with the lack of AOM biomarkers and high-molecular weight hydrocarbons in the carbonate concretions.

Petrographic identification of isopachous acicular aragonite cement in the carbonate concretions suggests that the seabed fluid flow in the study area is not the result of submarine discharge of freshwater from aquifers accessing the remote onshore Western Australia, or brines expelled from the porewaters of offshore sedimentary basins. If this were the case, then the cementing carbonate phase would be expected to comprise dolomite or calcite respectively. The results of the isotope analyses show a distinct but minor shift between the bulk ($\delta^{13}C$=4.01‰, $\delta^{18}O$=0.52‰) and cement ($\delta^{13}C$=3.46‰, $\delta^{18}O$=0.13‰) samples, with both sets of values plotting within the 'modern seawater' field on a stable isotope field diagram (cf. Campbell 2006). The slight difference between the isotopic values of the bulk and cement samples is interpreted to reflect differing ocean chemistry during the Pleistocene, when the oolites formed (James et al. 2004; Dix et al. 2005), relative to the Holocene, when the cement formed.

Multiple lines of evidence from isotopic, geochemical and petrographic analyses and acoustic datasets are consistent in effectively discounting any influence of methane or meteoric or basinal waters in the formation of the seabed fluid expulsion features. Furthermore, the isotopic results and presence of acicular aragonite as the cementing phase in the concretions suggest that the seeping fluids are normal marine seawater.

Assuming the seawater in the study area has normal saturation values for $CaCO_3$, the cementation of the concretions would have been dependent on the flux of seawater through the sediments, with each pore volume of seawater depositing a fraction of carbonate cement due to minor differences in the bicarbonate and calcium ion contents of the pore and bottom waters (Scholle and Halley 1985). Cementation is facilitated in areas where sediments are both porous and permeable, in high-energy settings, and in areas of low or restricted sedimentation rate (Shinn 1969; Moore 1989). The apparent porous and permeable nature of the oolitic sediment sampled in the grabs, the shallow macrotidal environment, and the age of the oolites (15.4–12.7 ka; James et al. 2004; Dix et al. 2005) suggest that these conditions exist in the study area, and that concretion formation may be linked to high rates of seawater flow across the sediment-water interface.

Model of pockmark development

This study has effectively demonstrated a spatial relationship between fluid expulsion pockmarks and a population of 'anomalous' (type II) sand waves. Sand waves which have unusual height-slope-length relationships ('freak' sand waves) have been suggested to be indicators of fluid seepage at a site in the southern North Sea (Fig. 11a; Hovland 1993; Judd and Hovland 2007). The 'anomalous' nature of the North Sea sand waves has been attributed to upwelling gas eroding sediment from adjacent to the sand waves. Despite the obvious morphological similarities between the North Sea sand waves and the sand waves in this study (Fig. 11), the processes linking the bedforms and fluid flow are interpreted to be entirely different. In this study, the 'anomalous' (type II) sand waves are more widely distributed than the evidence of fluid expulsion (pockmarks), which suggests that the nature of the bedforms may be a key contributing, but not the sole defining, factor in the development of the seabed fluid flow, rather than the anomalous bedforms being formed by fluid seepage. This is supported by indications that in the study area the fluid is seawater, not basinal fluids driven by geological processes as is the case in the North Sea (Hovland 1993; Judd and Hovland 2007).

There are two possibilities for the origin of the marine waters flowing from the seabed to form the pockmarks. The

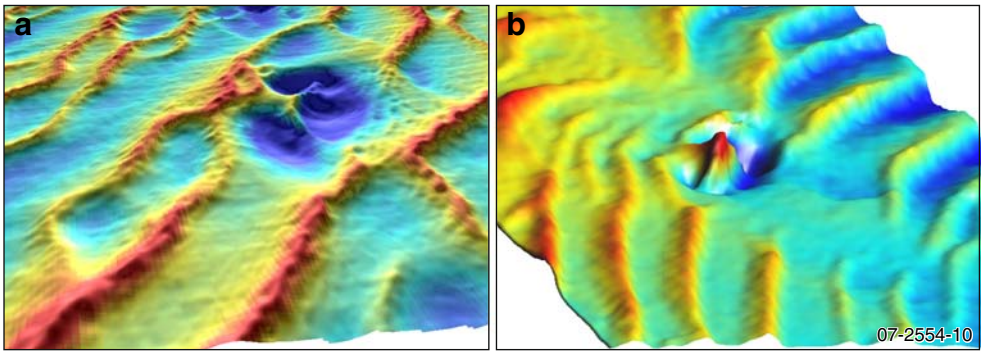

Fig. 11 **a** A sand wave with unusually high bedform height ('freak' sand wave) in the North Sea (Hovland 1993; Judd and Hovland 2007; image courtesy of A. Judd). Field of view facing approximately west. *Red and dark blue tones* correspond to 30 and 43 m water depth respectively. Spatial extent of scour around the sand wave approximately 400 m long and 100 m wide. **b** A type II sand wave from the present study area, appearing very similar to the North Sea sand wave. Field of view facing approximately southwest. *Red and dark blue tones* correspond to 100 and 116 m water depth respectively. Spatial extent of scour around the sand wave approximately 400 m long and 150 m wide

first is dewatering of near-surface sediments through rapid deposition of the type II sand waves, and the second is flow through the near surface driven by pressure gradients over the type II sand waves.

Harrington (1985) suggested that pockmarks in the central North Sea, of a scale similar to that of the pockmarks in the study area, were formed by porewater expulsion from compacting sediments. The initial phase of the dewatering mechanism for the North Sea pockmarks required build-up of porewater pressure in soft cohesive sediment (silt or clay). The very fine- to coarse-grained oolitic sands in the present study area would preclude this process, with relatively large pore throats enabling the release of porewater pressure through capillary flow. If the study area pockmarks formed through sediment compaction and porewater expulsion, then the initial phase of the dewatering mechanism may be associated with loading of near-surface sediments through rapid construction of the high-amplitude type II sand waves. However, fluid flow in the study area is unlikely to be due solely to an expulsion 'event' associated with rapid sediment loading, as this is not consistent with concretion formation, which requires significant flux of seawater through the pore spaces for cementation.

Seabed fluid flow in the study area may be driven by pressure gradients in the near surface. High-amplitude macrotides on this part of the shelf are the most likely mechanism for initiating a pressure differential at the seabed (i.e. tidal pumping), although atmospheric low-pressure systems and adjacent longshore oceanic currents are potential alternatives. In all submarine environments, water currents flowing near the sediment-water interface are deflected by seabed topography (Fig. 12). Flow obstruction by positive-relief seabed features causes a pressure increase over the slopes opposing the flow, and pressure decrease where the flow accelerates as it passes over the elevated structure (i.e. the Bernoulli principle; Batchelor 1967; Schlichting 1987). In permeable, unconsolidated sediments the resulting pressure gradients produce interstitial fluid flow through the near-surface sediments and across the sediment-water interface (Huettel and Gust 1992; Huettel et al. 1996). Tidal pumping over sand waves in Torres Strait has been demonstrated to drive seawater along connected permeability pathways in seabed sediments and form carbonate cements (Keene and Harris 1995), but this process has not previously been linked to fluid expulsion features.

A number of aspects of the marine geology and oceanography in the study area contribute to this site being a prime candidate for the development of relatively powerful fluid flow across the sediment-water interface and through the pores of near-surface sediments. The slopes of type II sand waves are unusually steep. The average type II sand wave slope is approximately 10° (maximum of 16.5°), whereas sand waves generally possess slopes of less than 10° and can slope as little as 1° (Allen 1982; Harris et al. 1986; Ashley et al. 1990). Interstitial flow increases considerably with increasing bedform slope, due to higher Bernoulli pressures (Shum and Sundby 1996); therefore, these steep sand waves would be more prone to inducing porewater flow (Fig. 12). Additionally, the seabed sediments are relict and appear to lack internal cross-stratification, which suggest that there is little overall net migration of the bedforms. Given this prolonged stability of the seafloor sediments, the porewater flows may have developed preferential migration pathways. Therefore, the interaction of the macrotidal currents and the high-amplitude type II sand waves may be contributing to relatively high pressure differentials adjacent to the sand waves, and consequent fluid flow development.

This hypothetical model is somewhat incongruous with the observation that pockmarks are not associated with all

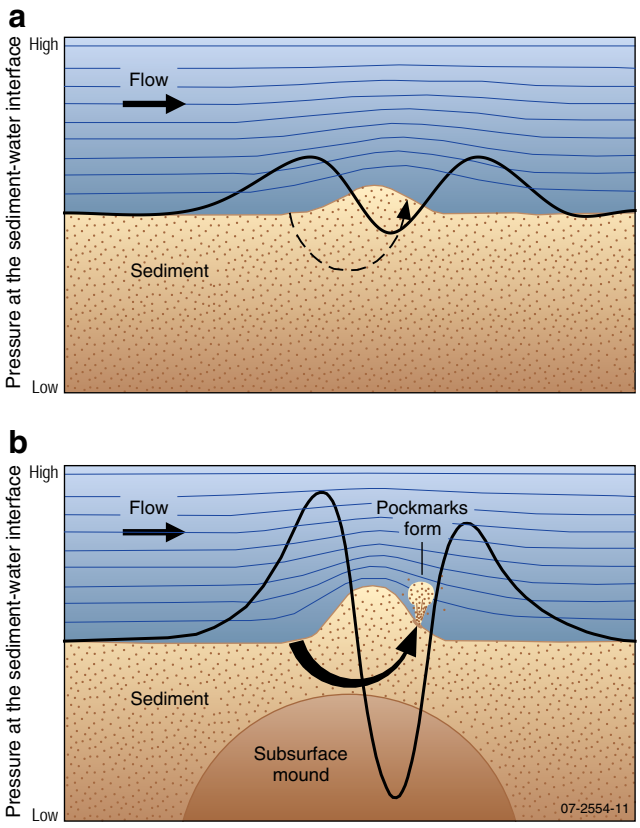

Fig. 12 Schematic conceptual model for porewater flows and seabed fluid expulsion features developed through interaction between currents and seabed topography. **a** Flow obstruction causes a pressure increase over the slopes opposing the flow, and the resulting pressure gradients produce interstitial fluid flow through the near-surface sediments. **b** High-amplitude sand waves contribute to relatively high pressure differentials, and fluid expulsion features form where the consequent fluid flow is confined and focused through a subsurface control

type II sand waves (Figs. 2, 3), given that tidal currents would be relatively uniform over such a small area of the shelf and would be expected to generate porewater flows at all steep, high sand waves. Sub-bottom profile data indicate that pockmarks may be spatially linked to type II sand waves which are located over 'mounds' in a shallow (near-surface) seismic reflector (Fig. 7). The depth of this reflector relative to the present sea level (~120 m) equates closely to the interpreted 120 m sea-level lowstand associated with the last glacial maximum (Chappell and Shackleton 1986). Therefore, this reflector may represent a palaeo-subaerial exposure surface, with exposure resulting in cementation and associated high amplitude. The topography on the reflector likely formed through deposition and erosion in a coastal system during the LGM lowstand. The spatial relationship between pockmarks, type II sand waves and subsurface reflector 'mounds' suggests that, while interstitial flows are generated through macrotidal currents flowing over type II sand waves, the confining and focusing of the porewater flows through this subsurface control may be required for fluid expulsion features to form (Fig. 12).

Testing of this hypothesis requires the acquisition of oceanographic and seabed acoustic data in the study area over time periods sufficient to capture the variability in sediment/current interactions and other influences such as storm and cyclone events.

Conclusions

This study represents the first documented evidence of seabed fluid flow in the central North West Shelf. This evidence includes seabed pockmarks which are roughly circular in shape and approximately 2–15 m in diameter, tubular and massive carbonate concretions, some of which line the surface of the pockmarks, and potential active venting of a fluid plume from the seabed.

The fluid which is flowing from the seabed is interpreted to be normal marine seawater, as indicated by oxygen and carbon isotope values for the bulk carbonate concretions and a sub-sample of acicular aragonite cement. This is supported by the isopachous acicular aragonite cement of the carbonate concretions, and the absence of vertical migration pathways and shallow gas indicators in the near-surface strata. Additionally, high-molecular weight petrogenic hydrocarbons and biomarker assemblages commonly found in methane-derived authigenic carbonate were not detected within any of the concretions.

The fluid flow features are located in association with type II sand waves which have atypical height-slope-length relationships. Seabed fluid flow across the sediment-water interface is interpreted to be the result of macrotidal currents flowing over the relatively steep slopes of the type II sand waves. Pockmarks and carbonate concretions develop where the interstitial flows are confined and focused by subsurface 'mounds' in a shallow seismic reflector.

The model developed in this study, describing the formation of fluid expulsion features through interactions between currents, bedforms and subsurface topography, is not endemic to Australia's North West Shelf, and could potentially be applied to other shallow sandy shelves with significant current flow. The model also has implications for future natural hydrocarbon seepage research. The identification of shallow gas signatures and fluid expulsion features in acoustic datasets (e.g. multibeam bathymetry and side-scan sonar) and visual observations (e.g. underwater video tows) are powerful tools for natural hydrocarbon seep exploration, but differentiating features as hydrocarbon- or non-hydrocarbon-related seeps requires judicial analysis and is most effective when supported by geochemical analysis.

Acknowledgements We thank the master and crew of the RV *Southern Surveyor*, CSIRO shipboard staff and Geoscience Australia staff for assistance with all aspects of data acquisition and interpretation throughout the survey. Chris Foudoulis is especially thanked for investigating and undertaking the separation of the aragonite cement from the ooids in the carbonate concretions. Michele Spinoccia and Bianca Reese are thanked for processing the multibeam swath bathymetry and drafting the figures respectively. We also thank Peter Harris, Phil O'Brien, Martin Hovland, Verner Ernstsen and Jens Greinert whose helpful reviews greatly improved the manuscript. This paper is published with the permission of the Chief Executive Officer, Geoscience Australia.

References

Allen JRL (1980) Sand waves: a model of origin and internal structure. Sed Geol 26:281–328

Allen JRL (1982) Sedimentary structures; their character and physical basis. Developments in Sedimentology 30A. Elsevier, Amsterdam

Aloisi G, Bouloubassi I, Heijs SK, Pancost RD, Pierre C, Sinninghe Damsté JS, Gottschal JC, Forney LJ, Rouchy J-M (2002) CH_4-consuming microorganisms and the formation of carbonate crusts at cold seeps. Earth Planet Sci Lett 203:195–203

Ashley GM, Boothroyd JC, Bridge JS, Clifton HE, Dalrymple RW, Elliot T, Flemming BW, Harms JC, Harris PT, Hunter RE, Kreisa RD, Lancaster N, Middleton GV, Payla C, Rubin DM, Smith JD, Southard JB, Terwindt JHT, Twichell DC Jr (1990) Classification of large-scale subaqueous bedforms: a new look at an old problem. J Sediment Petrol 60:160–172

Batchelor GK (1967) An introduction to fluid dynamics. Cambridge University Press, New York

Brunskill GJ, Burns KA, Opdyke B (2005) Biogeochemical processes, effects and signatures of hydrocarbon and ground-water seepage within a tropical, carbonate-rich system: Australia's Timor Sea. http://www.marine.csiro.au/nationalfacility/voyagedocs/2005/index.htm

Bucher WH (1919) On ripples and related sedimentary surface forms and their palaeogeographical interpretations. Am J Sci 47(149–210):241–269

Burnett WC, Bokuniewicz H, Huettel M, Moore WS, Taniguchi M (2003) Groundwater and pore water inputs to the coastal zone. Biogeochemistry 66:3–33

Butterfield DA (2000) Deep ocean hydrothermal vents. In: Sigurdsson H (ed) Encyclopaedia of volcanoes. Academic, New York, pp 857–875

Campbell K (2006) Hydrocarbon seep and hydrothermal vent paleoenvironments and paleontology: past developments and future research directions. Palaeogeogr Palaeoclimatol Palaeoecol 232:362–407

Chappell J, Shackleton NJ (1986) Oxygen isotopes and sea level. Nature 324:137–140

Díaz-del-Río V, Somoza L, Martínez-Frias J, Mata MP, Delgado A, Hernandez-Molina FJ, Lunar R, Martín-Rubí JA, Maestro A, Fernández-Puga MC, León R, Llave E, Medialdea T, Vázquez JT (2003) Vast fields of hydrocarbon-derived carbonate chimneys related to the accretionary wedge/olistostrome of the Gulf of Cádiz. Mar Geol 195:177–200

Dix GR, James NP, Kyser TK, Bone Y, Collins LB (2005) Genesis and dispersal of carbonate mud relative to late quaternary sea-level change along a distally-steepened carbonate ramp (Northwestern Shelf, Western Australia). J Sediment Res 75:665–678

Dugan B, Flemings PB (2000) The New Jersey margin: compaction and fluid flow. J Geochem Explor 69(70):477–481

Dugan B, Flemings PB (2002) Fluid flow and stability of the US Continental Slope offshore New Jersey from the Pleistocene to the present. Geofluids 2:137–146

Elvert M, Suess E, Greinert J, Whiticar MJ (2000) Archaea mediating anaerobic methane oxidation in deep-sea sediments at cold seeps of the eastern Aleutian subduction zone. Org Geochem 31:1175–1187

Fenster MS, Fitzgerald DM, Moore MS (2006) Assessing decadal-scale changes to a giant sand wave field in eastern Long Island Sound. Geology 34:89–92

Flemming BW (1988) Zur Klassifikation subaquatischer, strömungstransversaler Transportkörper. Bochumer Geol Geotechnol Arb 29:44–47

Fyfe WS (1994) The water inventory of the Earth: fluids and tectonics. In: Parnell J (ed) Geofluids: origin, migration and evolution of fluids in sedimentary basins. Geol Soc Lond Spec Publ 78:1–7

Harrington PK (1985) Formation of pockmarks by pore-water escape. Geo-Mar Lett 5:193–197. doi:10.1007/BF02281638

Harris PT, Ashley GM, Collins MB, James AE (1986) Topographic features of the Bristol Channel sea-bed: a comparison of SEASAT (synthetic aperture radar) and side-scan sonar images. Int J Remote Sens 7:119–136

Harvey JG (1966) Large sand waves in the Irish Sea. Mar Geol 4:49–55

Hovland M (1993) Submarine gas seepage in the North Sea and adjacent areas. In: Parker JR (ed) Petroleum geology of Northwest Europe. Proc 4th Conf, Geological Society, London, pp 1333–1338

Hovland M, Judd AG (1988) Seabed pockmarks and seepages. Graham and Trotman, London

Huettel M, Gust G (1992) Impact of bioroughness on interfacial solute exchange in permeable sediments. Mar Ecol Prog Ser 89:253–267

Huettel M, Ziebis W, Forster S (1996) Flow-induced uptake of particulate matter in permeable sediments. Limnol Oceanogr 41:309–322

Hulscher SJMH (1996) Tidal induced large-scale regular bed form patterns in a three-dimensional shallow water model. J Geophys Res 101(C9):20727–20744

Hulscher SJMH, Van den Brink GM (2001) Comparison between predicted and observed sand waves and sandbanks in the North Sea. J Geophys Res 106(C5):9327–9338

James NP, Bone Y, Kyser TK, Dix GR, Collins LB (2004) The importance of changing oceanography in controlling late Quaternary carbonate sedimentation on a high-energy, tropical, oceanic ramp: north-western Australia. Sedimentology 51:1179–1205

Jones HA (1973) Marine geology of the northwestern Australian continental shelf. BMR Bull 136

Jones AT, Logan GA, Kennard JM, Rollet N (2005a) Reassessing potential origins of synthetic aperture radar (SAR) slicks from the Timor Sea region of the North West Shelf on the basis of field and ancillary data. APPEA J 45:311–331

Jones AT, Logan GA, Kennard JM, O'Brien PE, Rollet N, Sexton M, Glenn KC (2005b) Testing natural hydrocarbon seepage detection tools on the Yampi Shelf, northwestern Australia, Geoscience Australia survey S267—post-survey report. Geoscience Australia Record 2005/15

Jones AT, Kennard JM, Ryan GJ, Bernadel G, Earl KL, Rollet N, Grosjean E, Logan GA (2007) Geoscience Australia marine survey SS06/2006 post-survey report: natural hydrocarbon seepage survey on the central North West Shelf. Geoscience Australia Record 2007/21

Judd AG, Hovland M (2007) Seabed fluid flow: The impact on geology, biology and the marine environment. Cambridge University Press, New York

Keene JB, Harris PT (1995) Submarine cementation in tide-generated bioclastic sand dunes: epicontinental seaway, Torres Strait, north-east Australia. Spec Publ Int Assoc Sediment 24:225–236

Land LA, Paull CK (2000) Submarine karst belt rimming the continental slope in the Straits of Florida. Geo-Mar Lett 20:123–132. doi:10.1007/s003670000041

Land LA, Paull CK, Hobson B (1995) Genesis of a submarine sinkhole without subaerial exposure: Straits of Florida. Geology 23:949–951

Martínez JI, De Deckker P, Barrows TT (1999) Palaeoceanography of the last glacial maximum in the eastern Indian Ocean: planktonic foraminiferal evidence. Palaeogeogr Palaeoclimatol Palaeoecol 147:73–99

McCave IN (1971) Sand waves in the North Sea off the coast of Holland. Mar Geol 10:199–225

Moore CH (1989) Carbonate diagenesis and porosity. Developments in sedimentology 46. Elsevier, Amsterdam

Németh AA, Hulscher SJMH, de Vriend HJ (2002) Modelling sand wave migration in shallow shelf seas. Cont Shelf Res 22:2795–2806

Németh AA, Hulscher SJMH, van Damme RMJ (2004) Modelling sand wave migration and height, comparing model results with data. In: Hulscher S, Garlan T, Idier D (eds) Int Worksh marine sandwave and river dune dynamics II, 1–2 April 2004. University of Twente, The Netherlands, pp 232–239

Németh AA, Hulscher SJMH, van Damme RMJ (2007) Modelling offshore sand wave evolution. Cont Shelf Res 27:713–728

Pape T, Blumenberg M, Seifert R, Egorov VN, Gulin SB, Michaelis W (2005) Lipid geochemistry of methane-seep-related Black Sea carbonates. Palaeogeogr Palaeoclimatol Palaeoecol 227:31–47

Paull C, Ussler W, Maher N, Greene HG, Rehder G, Lorenson T, Lee H (2002) Pockmarks of Big Sur, California. Mar Geol 181:323–335

Reitner J, Peckmann J, Blumenberg M, Michaelis W, Reimer A, Thiel V (2005) Concretionary methane-seep carbonates and associated microbial communities in Black Sea sediments: geobiology of ancient and modern methane-seeps. Palaeogeogr Palaeoclimatol Palaeoecol 227:18–30

Rollet N, Logan GA, Kennard JM, O'Brien P, Jones AT, Sexton M (2006) Characterisation and correlation of active hydrocarbon seepage using geophysical data sets: an example from the tropical, carbonate Yampi Shelf, Northwest Australia. Mar Petrol Geol 23:145–164

Rollet N, Logan GA, Ryan G, Judd AG, Totterdell JM, Glenn K, Jones AT, Kroh F, Struckmeyer HIM, Kennard JM, Earl KL (2009) Shallow gas and fluid migration in the northern Arafura Sea (offshore Northern Australia). Mar Petrol Geol 26:129–147

Schlichting H (1987) Boundary layer theory, 7th edn. McGraw-Hill, New York

Scholle PA, Halley RB (1985) Burial diagenesis: out of sight, out of mind. In: Schneidermann N, Harris PM (eds) Carbonate cements. SEPM Spec Publ 36:309–334

Shinn EA (1969) Submarine lithification of Holocene carbonate sediments in the Persian Gulf. Sedimentology 12:109–144

Shum KT, Sundby B (1996) Organic matter processing in continental shelf sediments—the subtidal pump revisited. Mar Chem 53:81–87

Taniguchi M, Burnett WC, Cable JE, Turner JV (2002) Investigation of submarine groundwater discharge. Hydrol Process 16:2115–2129

Terwindt JHJ (1971) Sand waves in the Southern Bight of the North Sea. Mar Geol 10:51–67

Thiel V, Peckmann J, Richnow HH, Luth U, Reitner J, Michaelis W (2001) Molecular signals for anaerobic methane oxidation in Black Sea seep carbonates and a microbial mat. Mar Chem 73:97–112

Van Veen J (1935) Sand waves in the North Sea. Hydrogr Rev 12:21–29